Polymer Journal

REGULAR ARTICLE

Kinetics of Living Anionic Polymerization of Polystyrenyl Lithium in Cyclohexane

*By Eri MISHIMA, Yumi MATSUMIYA, Shigeru YAMAGO, and Hiroshi WATANABE**

Living anionic polymer chains polymerized with organolithium initiators usually form aggregates through their Li ends in nonpolar solvents. This aggregation structure strongly affects the anionic polymerization (propagation) kinetics. In the conventional molecular picture, the aggregates are assumed to be chemically inert and the propagation occurs only though the dissociated unimers, which leads to single-exponential decay of the residual monomer fraction $\phi(t)$ with time t. This picture was tested by ^{1}H NMR measurements for protonated polystyrenyl lithium (hPSLi) polymerized in a nonpolar solvent, deuterated cyclohexane (dCH). The measurements were made mostly at 34.5 °C, the theta condition for neutral (non-anionic) high-M hPS. An oligomeric, deuterated styrenyl lithium (oSLi) was utilized as an initiator so that the NMR data exclusively detected the propagation kinetics (no contamination of the initiation process). For hPSLi with the molecular weight ranging from 4.2×10^3 to 276×10^3, $\phi(t)$ was found to exhibit almost single-exponential decay at short t (where $\phi(t) > 10$–20%) but the decay slowed at longer t (for smaller $\phi(t)$). Furthermore, $\phi(t)$ decayed more slowly when the polymerization batch contained neutral, deuterated dPS (not affecting the hPSLi chemistry) at a concentration in the semi-dilute regime. These results indicated the failure of the conventional molecular picture assuming the chemical inertness of the aggregates. Consequently, some (unstable) aggregates appeared to contribute to the propagation, and the osmotic interaction among the aggregates as well as with the coexisting dPS seemed to reduce this contribution at long t thereby giving the non-single-exponential decay of $\phi(t)$. A simple kinetic model considering this osmotic effect consistently described the behavior of $\phi(t)$ in the absence/presence of dPS for the polymerization of hPS in a range of $10^{-3}M = 11$–73, although deviations were noted for the polymerization of lower- and higher-M hPS.

KEY WORDS: Anionic Polymerization Kinetics / Polystyrenyl Lithium / Aggregates / Osmotic Effect /

The living anionic polymerization utilizing organolithium (RLi) molecules as the initiator in nonpolar solvents offers an important route of synthesizing well characterized, narrow molecular weight distribution (MWD) polymers such as polydiene rubbers of high 1–4 linkage content.[1–4] The anionic polymerization kinetics and the structures of the initiators/anionic chains have been extensively studied partly because of this importance.[1–22] These studies revealed that the RLi initiator molecules form aggregates in nonpolar solvents and thus the simplest initiation kinetics ($RLi + M \rightarrow RM^-Li^+$; M = monomer) does not hold, although the effect of the aggregation on the initiation has not been fully understood yet.[4,11,15,16]

The aggregation occurs not only for the initiators but also for the polymerized anionic chains in nonpolar solvents. Scattering/viscosity experiments revealed that the anionic chains form aggregates with the main aggregation number f being determined by the chemistry of the anionic ends:[1–4,7,12,16–22] For example $f = 2$ for polystyrenyl lithium chains in the range of the molecular weight $10 < 10^{-3}M < 200$. The aggregation number has a distribution (for example, ranging mainly from 3 to 5 for polybutadienyl lithium in cyclohexane)[21] and a trace amount of huge aggregates (with the aggregation number ≥ 100) coexists with smaller aggregates.[16–22] This aggregation structure has a pronounced effect on the propagation process after full consumption of the initiator.

For the propagation process, a simple molecular picture shown in Scheme 1 has been conventionally accepted as the governing kinetics.[1–4] This picture assumes that the chemical equilibrium between the main f-mer aggregates and the dissociated unimer chains is largely shifted toward the former and the propagation occurs only through the latter. (The aggregates are stabilized through Li-Li bonds therein and thus assumed to be chemically inert compared to the unimers). This assumption leads to a simple kinetic equation for the molar concentration of the monomer [M],

$$\frac{d[M]}{dt} = -k_1[P_1][M] \tag{1}$$

where k_1 and $[P_1]$ denote the propagation rate constant and molar concentration of the unimer. The large shift of the equilibrium toward the f-mer aggregates allows an approximation,

$$K_f = \frac{[P_1]^f}{[P_f]} \cong \frac{[P_1]^f}{\{[I]_0/f\}} \tag{2}$$

Here, $[P_f]$ and K_f are the molar concentration of the f-mer aggregates and the equilibrium constant (*cf.* Scheme 1), respectively, and $[I]_0$ is the molar concentration of the initiator

Institute for Chemical Research, Kyoto University, Uji 611-0011, Japan
*To whom correspondence should be addressed (Tel: +81-774-38-3135, Fax: +81-774-38-3139, E-mail: hiroshi@scl.kyoto-u.ac.jp).

$$(\mathrm{PLi})_f \underset{}{\overset{K_f}{\rightleftharpoons}} f\mathrm{PLi}$$

$$\mathrm{PLi} + \mathrm{M} \xrightarrow[k_1]{} \mathrm{PLi}$$

Scheme 1. Conventionally accepted route of propagation through dissociated unimer chains.

(= total molar concentration of the anionic chains). Eqs 1 and 2 lead to a single-exponential decay of the residual fraction of the monomer $\phi(t)$ during the propagation process,[1–4]

$$\phi(t) \equiv \frac{[\mathrm{M}]}{[\mathrm{M}]_0} = \exp\left(-\frac{t}{\tau}\right) \text{ with } \tau = \frac{1}{k_1}\left(\frac{f}{K_f[\mathrm{I}]_0}\right)^{1/f} \quad (3)$$

with $[\mathrm{M}]_0$ and t being the monomer concentration at the onset of the propagation and a time after this onset, respectively. Most of the kinetic experiments[1–5,8,9,13,14] lent support to this single-exponential decay, though only in an early stage of the propagation (at short t).

However, a ^{7}Li NMR experiment[22] for living polybutadienyl lithium (PBLi) chains posed a question for the chemical inertness of the aggregates. For PBLi mainly forming tetrameric aggregates in benzene,[21,22] the NMR data indicated that a thermal exchange of several different Li species occurs in the system and its characteristic time τ_{ex} depends on the concentration (C) and molecular weight (M) of PBLi.[22] This τ_{ex} was associated with an activation energy ($\Delta E = 88\,\mathrm{kJ\,mol^{-1}}$) considerably lower than the energy $\Delta E_{\mathrm{C\text{-}Li}}$ for a C-Li bond dissociation[23] ($> 150\,\mathrm{kJ\,mol^{-1}}$). The C- and M-dependencies of τ_{ex} as well as this ΔE value suggested that the Li-Li exchange occurs mainly through a thermal fusion of the tetrameric aggregates into larger aggregates without forming the dissociated unimers.[22] These fused aggregates should be less stable and thus in a *higher energy state* compared to the tetrameric aggregates (detected in scattering experiments[21,22] as the main component of the aggregates), suggesting a possibility that the fused aggregates, once formed transiently, contribute to the propagation. This possibility is in harmony with quantum chemistry calculations[23,24] that suggest a low probability of the propagation only through the dissociated unimers.

Following the above results, we recently made ^{1}H NMR experiments to examine the propagation kinetics of PBLi (with $10^{-3}M = 8.6$–26.3) in benzene (Bz).[25] The residual monomer fraction $\phi(t)$ was found to exhibit the single-exponential decay only in the early stage of propagation where $\phi(t) > 10\%$, and the decay of $\phi(t)$ became slower in the late stage.[25] (This non-single-exponential behavior was not observed in the previous studies[1–5,8,9,13,14] simply because these studies traced $\phi(t)$ only in the early stage.) Furthermore, the decay was retarded in the presence of chemically inert, neutral (non-anionic) PB chains.[25] These results unequivocally indicated that the conventional molecular picture, shown in Scheme 1 and eq 3, does not accurately hold for the PBLi/Bz systems.

In relation to this point, we note that the single-exponential decay *should* be observed even when the fused aggregates contribute to the propagation *if the equilibrium constants among all kinds of aggregates are independent of* $\phi(t)$. Thus, the equilibrium constants in the PBLi system should have changed with $\phi(t)$, which led to a hypothesis that this change results from the osmotic interaction of the aggregates (that tends to suppress the fused aggregate formation). A simple analysis incorporating this osmotic effect was in harmony with the measured $\phi(t)$ data, which lent support to this hypothesis.[25]

This osmotic effect cannot be unique to the PBLi system but is expected for all living anionic polymerization systems in nonpolar solvents. Thus, we tested this effect through ^{1}H NMR measurements for polystyrenyl lithium (PSLi) polymerized in cyclohexane (CH) at 34.5 °C (= theta temperature for neutral high-M PS chains) and other temperatures. The $\phi(t)$ data obtained for the PSLi/CH systems showed the non-single-exponential decay and this decay was retarded in the presence of neutral PS, as similar to the behavior of the PBLi/Bz systems. In addition, the $\phi(t)$ data of the PSLi/CH systems were considerably well described by a simple kinetic model incorporating the osmotic effect (expressed in terms of the osmotic pressure data for PS in CH[26]). Details of these results are described in this paper.

EXPERIMENTAL

Materials and Sample Preparation

Protonated and deuterated styrene monomers (hS and dS; purchased from Tokyo Kasei and Aldrich, respectively), deuterated cyclohexane (dCH; Aldrich), heptane (Wako), benzene (Wako), deuterated *sec*-butyl chloride (Cambridge Isotope Lab), and methanol (Wako) were purified with the standard methods.[1] All chemical reactions were made in glass ampoules/flasks with the aid of the standard high vacuum technique using glass constrictions and breakable seals.

Deuterated *sec*-butyllithium (dBuLi) was synthesized from Li metal (Aldrich) and deuterated *sec*-butyl chloride in heptane. Oligomeric styrenyl lithium (oSLi) was synthesized from dS monomer and dBuLi in benzene (Bz) at 40 °C, and its characteristics ($M_w = 1.4 \times 10^3$, $M_w/M_n = 1.10$) were determined with time-of-flight mass spectroscopy as explained later. After the synthesis, the solvent for oSLi was switched from Bz to dCH through vacuum evaporation (of Bz) and distillation (of dCH).

A deuterated polystyrene (dPS), utilized as an additive for polymerization batches of protonated polystyrenyl lithium (hPSLi), was anionically synthesized from dBuLi and dS monomer in Bz at room temperature. The resulting dPSLi anions were terminated/precipitated in large excess of methanol and the supernatant methanol/Bz phase was removed by decantation. The remaining dPS was dissolved in Bz and then precipitated again in excess methanol, and the supernatant was removed by decantation. After this dissolution/precipitation procedure repeated for three times in vacuum, dPS was thoroughly dried with the aid of a high vacuum line and dissolved in dCH. A small amount of oSLi was added to this dPS/dCH solution to purge impurities (terminators for living anions) therein. After addition of just enough amount of oSLi, the solution exhibited pale yellow color (color of very dilute

Polymer Journal

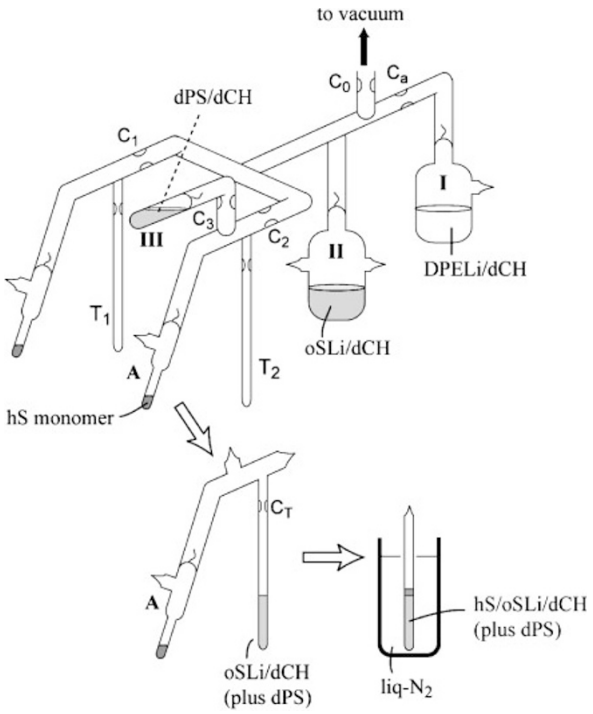

Figure 1. Schematic illustration of a glass apparatus for preparation of hS/oSLi/dCH and hS/oSLi/dPS/dCH solutions sealed in NMR test tubes. For simplicity, magnetic bars utilized for opening the breakable seals are not shown.

oSLi). Then, the dPS/CH solution was split into several ampoules and stored in a deep freezer until use. The molecular characteristics of the dPS sample, $M_w = 56.8 \times 10^3$ and $M_w/M_n = 1.05$, were determined from GPC as explained later.

The materials subjected to the NMR measurements were the anionically polymerizing hS/oSLi/dCH solutions sealed in NMR test tubes made of glass (diameter = 5 mm). Some batches also contained chemically inert dPS (prepared as above) that tuned the osmotic environment for the propagating hPSLi chains. A glass apparatus utilized for sealing these solutions in the NMR tubes is schematically shown in Figure 1. (The design of this apparatus was similar but not identical to that used in the previous study.[25]) For simplicity of Figure, magnetic bars for opening the breakable seals are not shown.

The apparatus was fully evacuated and then sealed at the constriction C_0. Impurities on the inside wall of the apparatus was purged with a dCH solution of diphenylethylenyl anion (DPELi; $CH_3CH_2CH(CH_3)CH_2C(C_6H_5)_2Li$) in the ampoule I. (This anion was separately made through reaction of DPE and *sec*-butyllithium.) Then, the DPELi solution was recovered in the ampoule I, the apparatus wall was thoroughly rinsed with dCH distilled from the ampoule I, and the ampoule I was sealed off at the constriction C_a. This sealing operation was made after cleaning the constriction C_a with dCH distilled thereto. (The cleaning operation was similarly made whenever necessary in the whole procedure of synthesis.)

After removal of the ampoule I, the oSLi/dCH solution was poured from the ampoule II into the NMR tubes, T_1 and T_2. The ampoule III containing the purified dPS/dCH solution ($\sim 0.8\,cm^3$) was attached to the stem for T_2 but not to the stem for T_1. After 0.1–0.7 cm^3 of the oSLi/dCH solution was poured into each NMR tube (with this volume being chosen according to the target molecular weight of hPSLi), the solution volume in T_1 was adjusted to be $\sim 0.5\,cm^3$ *via* vacuum distillation/removal of dCH from/into the ampoule II, and the stem carrying T_1 was sealed off at the constriction C_1. Most of the solvent dCH in T_2 was carefully distilled back to the ampoule II to leave a concentrated oSLi/dCH solution in T_2, and the stem carrying T_2 was sealed off at the constriction C_2. Then, the dPS/dCH solution ($\sim 0.8\,cm^3$) was poured from the ampoule III into T_2 to dilute oSLi in T_2. Finally, the volume of the oSLi/dPS/dCH solution in T_2 was adjusted to be $\sim 0.5\,cm^3$ by distilling dCH back to the ampoule III, and the ampoule III was sealed off at the constriction C_3.

With the above procedure, we successfully prepared pairs of oSLi/dPS/dCH solutions of roughly the same oSLi concentration but different dPS concentrations (zero concentration in T_1) sealed in separate NMR tubes. The hS monomer (typically 0.02–0.07 cm^3; contained in the ampoule A) was distilled into the NMR tube chilled with liquid nitrogen (liq-N_2) and then the tube was sealed off at the constriction C_T. The oSLi/dPS/dCH solution and hS monomer thus sealed in the tube were kept frozen in liq-N_2 until they were subjected to the NMR measurement. Just before the measurement, they were allowed to quickly melt and mix with each other at room temperature and then the tube containing this mixture was quickly set in the NMR spectrometer to start the polymerization experiment.

Measurements

NMR. For the hS/oSLi/dCH and hS/oSLi/dPS/dCH solutions in the NMR tubes kept at a constant temperature (= 34.5 °C for most cases and 28 °C and 45 °C for some cases) in Varian MERCURYplus AS400 spectrometer, the concentration of hS monomer during the polymerization (propagation) was monitored through ^1H NMR measurements. A static magnetic field was set at 9.4 T, and the resonance frequency was 400.0 MHz. The pulse width (flip angle), pulse repetition, and number of scan were 6.25 μs (90 deg), 1 min, and 4, respectively. The measurement was conducted until the fraction of the residual monomer $\phi(t)$ decreased to ~3% (*i.e.*, up to the conversion of ~97%). The measured ^1H chemical shift was expressed as the value relative to a signal from tetramethylsilane (separately measured in deuterated chloroform).

The ^1H NMR data were recorded as a function of the time t from the onset of propagation (when the hS/oSLi/dCH and/or hS/oSLi/dPS/dCH solutions were allowed to quickly mix). The ^1H spectra detected the concentration of various ^1H species. Figure 2 shows an example of the ^1H spectra obtained during the polymerizing process of hPS in the presence of dPS (at $t = 36$ min for a batch 16(0.05, 0.10) explained later). Separated ^1H signals from the CH_2 and C_6H_5 groups of the hS monomer and the polymerized hPS are clearly observed without being disturbed by the deuterated dCH, dPS, and the oligomeric fragment of the initiator (the oS part from oSLi).

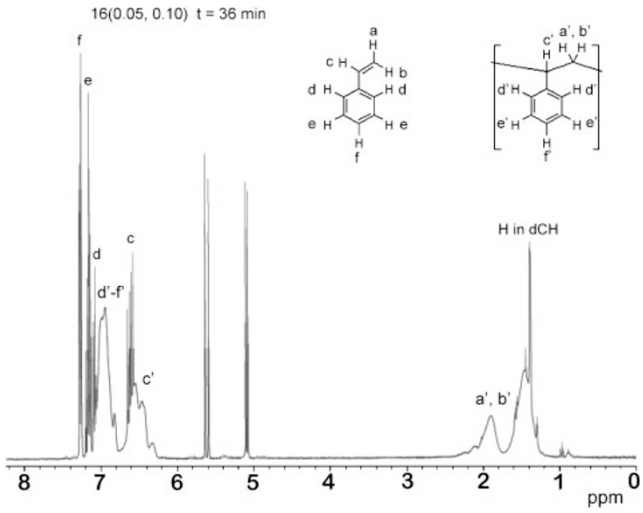

Figure 2. ^{1}H NMR spectrum of polymerization batch 16(0.05, 0.10) at $t = 36$ min.

From the integrated intensities I of these signals at respective times t, we evaluated the residual fraction of the hS monomer, $\phi(t) = I_{\text{monomer}}/(I_{\text{monomer}} + I_{\text{hPS}})$. The $\phi(t)$ values evaluated from the CH_2 and C_6H_5 signals agreed with each other.

After full conversion of the propagation (achieved by keeping the NMR tubes, after the above measurement, at room temperature for ~ 1 d), ^{7}Li NMR measurements were conducted for some batches at several temperatures with a JEOL JNM-AL400 spectrometer. A static magnetic field was set at 9.4 T, and the resonance frequency was 153.86 MHz. The pulse width (flip angle), pulse repetition, and number of scan were 7.2 μs (45 deg), 0.5 min, and 6400 (or 4096 for a few cases), respectively. The measured ^{7}Li spectra, expressed as the value relative to a 0.2 M $LiCl/D_2O$ solution (reference system), reflected the rate of the Li-Li exchange between the polymerized hPSLi chains.

Concentration Determination and Material Characterization After completion of the polymerization in the NMR tube, the tube was opened in an atmosphere of methanol vapor to terminate the living hPSLi therein. Then, the dCH solution of hPS (hPS plus dPS for some batches) was recovered in a clean glass jar, and the masses m_b and m_a of the solution before and after thorough evaporation of dCH were measured. The meniscus line of the solution was marked on the NMR tube before it was opened and, after cleaning the inside of the tube, the volume of the solution V_s was determined as a volume of water filled up to this line. (The water volume was calculated from the water mass and the density, $d_{\text{water}} = 1.00\,\text{g cm}^{-3}$). The total PS concentration in the polymerization solution (in mass/volume unit) was evaluated as

$$C = m_a/V_s \tag{4a}$$

$$C = m_a/\{(m_b - m_a)d_{\text{dCH}}^{-1} + m_a w_{\text{hPS}} d_{\text{hPS}}^{-1} + m_a(1 - w_{\text{hPS}})d_{\text{dPS}}^{-1}\} \tag{4b}$$

Here, d_{dCH} ($= 0.89\,\text{g cm}^{-3}$),[27] d_{hPS} ($= 1.05\,\text{cm}^{-3}$),[28] and d_{dPS} ($= 1.12\,\text{cm}^{-3}$)[29] are the densities of dCH, hPS, and dPS, respectively, and w_{hPS} is the hPS weight fraction in the hPS/dPS mixture recovered after full evaporation of dCH. (The w_{hPS} value was determined from the GPC data explained later.) The concentration evaluated with eq 4b (under an assumption of volume additivity) agreed well with that evaluated with eq 4a.

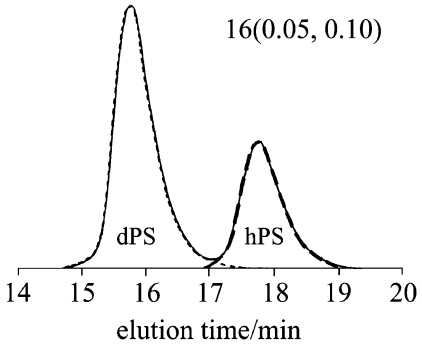

Figure 3. GPC profile of batch 16(0.05, 0.10) on completion of polymerization (thin solid curve). Dashed and dotted curves indicate the profiles of hPS and coexisting dPS, respectively.

The hPS samples recovered from the polymerization batches containing no dPS were straightforwardly characterized with GPC (CO-8020 and DP-8020, Tosoh). The eluent was tetrahydrofuran (THF), and monodisperse linear PS standards (TSK's, Tosoh) were utilized to calibrate the elution volume.

The GPC characterization was conducted also for the dPS sample, the non-reactive additive in the polymerization batches. The results were $M_w = 56.8 \times 10^3$ and $M_w/M_n = 1.05$. The GPC profile of the dPS sample was utilized in the characterization of the hPS sample recovered from the polymerization batches containing dPS, as explained below.

Figure 3 shows an example of the GPC profile (thin solid curve) for the mixtures of hPB and dPB recovered from such a batch (16(0.05, 0.10) explained later). The hS monomer/initiator molar ratio in the polymerization batches was adjusted in a way that the fully polymerized hPS had a molecular weight considerably smaller than that of dPS. Thus, the GPC profiles of all hPS/dPS mixtures had well-separated two peaks, and the profile around the dPS peak agreed well with the known profile for dPS; see the dotted curve in Figure 3. The GPC profile of the hPS sample (thick dashed curve) was easily evaluated by subtracting the dPS profile from the raw profile (thin solid curve) and the hPS sample was characterized with this subtracted profiles. In addition, the hPS weight fraction w_{hPS} in the hPS/dPS mixture was evaluated from the ratio of the GPC peak areas for hPS and dPS after a correction for the difference of the hPS and dPS densities.

The initiator, oligomeric styrenyl lithium (oSLi), was characterized with time-of-flight mass spectroscopy (TOFMS) utilizing a spectrometer (Applied Biosystems Voyage TM DE-STR/JK). The results were $M_w = 1.4 \times 10^3$ and $M_w/M_n = 1.10$. This initiator molecular weight was utilized to convert the residual hPS monomer fraction $\phi(t)$ at time t during the propagation process to the hPS molecular weight/concentration at that t.

Table I. Characteristics of hPS samples and polymerizing condition

Code[a]	$10^{-3}M_{hPS}(\infty)$[b]	$[M_w/M_n]_{hPS}$	$C_{hPS}(\infty)$[c]/g cm^{-3}	C_{dim}*[d]/g cm^{-3}	$10^6[I]_0$[e]/mol cm^{-3}	C_{dPS}[f]/g cm^{-3}
			polymerized at 34.5 °C			
4(0.02, 0)	4.2	1.04	0.020	0.166	5.0	0
11(0.05, 0)	11.4	1.04	0.046	0.101	4.2	0
16(0.13, 0)	15.7	1.04	0.130	0.086	8.6	0
36(0.01, 0)	36.2	1.04	0.013	0.057	0.39	0
71(0.05, 0)	70.5	1.07	0.048	0.041	0.71	0
73(0.13, 0)	73.2	1.05	0.125	0.040	1.8	0
148(0.11, 0)	148	1.10	0.106	0.028	0.79	0
276(0.04, 0)	276	1.16	0.038	0.021	0.16	0
13(0.07, 0.09)	13.2	1.05	0.068	0.094	5.4	0.086
14(0.08, 0.03)	13.9	1.05	0.084	0.092	6.3	0.025
16(0.05, 0.10)	16.0	1.05	0.045	0.085	3.0	0.104
17(0.09, 0.10)	17.3	1.05	0.091	0.082	5.5	0.103
			polymerized at 28 °C			
12(0.04, 0)	12.1	1.04	0.036	0.098	3.1	0
10(0.06, 0.11)	9.7	1.04	0.064	0.109	6.9	0.114
			polymerized at 45 °C			
16(0.05, 0)	15.5	1.05	0.053	0.086	3.6	0
9(0.04, 0.10)	8.7	1.03	0.044	0.115	5.2	0.099

a: First number in the code indicates the hPS molecular weight (in unit of 1000) on completion of the polymerization. First and second numbers in the parenthesis represent the concentrations of hPS and dPS (with the former referring to the concentration on completion of polymerization). b: Weight average molecular weight of hPS on completion of polymerization. c: Concentration of hPS on completion of polymerization. d: Overlapping concentration of linear dimers of hPSLi on completion of polymerization. e: Initiator concentration f: Concentration of dPS ($M_w = 56.8 \times 10^3$, $M_w/M_n = 1.05$): The dPS chains, when existing, had the concentrations larger than their overlapping concentration, $C_{dPS}^* = 0.066\,g\,cm^{-3}$, *except in the batch 14(0.08, 0.03).*

Table I summarizes the characteristics of the hPS samples and their polymerization conditions. The first number in the code indicates the hPS molecular weight $M_{hPS}(\infty)$ (in unit of 1000) on completion of the polymerization, and the first and second numbers in the parenthesis represent the hPS and dPS concentrations $C_{hPS}(\infty)$ and C_{dPS} (in g cm^{-3} unit), with the former referring to the concentration on completion of polymerization. When dPS was added to the polymerization batch, its C_{dPS} was chosen to be below 0.12 g cm^{-3} but above its overlapping concentration, $C_{dPS}^* = 0.066\,g\,cm^{-3}$ (calculated from the data[30] for the radius of gyration R_g of hPS in CH at 34.5 °C, $R_g/cm = 3.0 \times 10^{-9}M^{1/2}$), except for the batch 14(0.08,0.03) having $C_{dPS} < C_{dPS}^*$. Namely, the solutions containing dPS (except 14(0.08,0.03)) were in the semi-dilute state throughout the polymerization (propagation) process. Table I also shows the initiator concentration $[I]_0$ (calculated from $C_{hPS}(\infty)$, $M_{hPS}(\infty)$, and $[M_w/M_n]_{hPS}$) and the overlapping concentration C_{dim}^* of the linear *dimeric* aggregates of hPSLi on completion of the polymerization (calculated from the R_g data of hPS in CH).

RESULTS AND DISCUSSION

Propagation in Solutions in the Absence of dPS

For the polymerization batches containing no dPS (*cf.* Table I), Figure 4 shows dependence of logarithm of the residual monomer faction $\phi(t)$ at 34.5 °C on the polymerization time t. In Figure 5, the same $\log\phi(t)$ data are reduced by the polymerization time t, magnified by a factor X as indicated, and plotted against t. In both Figures 4 and 5, the curves indicate the results of calculation with a kinetic model explained later. Since the oligomeric oSLi was utilized as the initiator, the decay of $\phi(t)$ data with t is exclusively attributed to the propagation process (no contribution from the initiation reaction of hS monomer with dBuLi).

As noted in Figure 4, $\phi(t)$ exhibits approximately single-exponential decay with t in the early stage of propagation at short t (where $\phi(t)$ remains larger than 10–20%). However, in the late stage at long t, the decay rate of $\log\phi(t)$ becomes smaller (and the $\log\phi(t)$ *vs* t plots has concave shape) in the batches having fairly large $C_{hPS}(\infty)$, which demonstrates the non-single-exponential feature of the whole propagation process. This non-exponential behavior is most clearly observed in Figure 5 as the increase of the $\{\log\phi(t)\}/t$ ratio with t for the batches having fairly large $C_{hPS}(\infty)$: Note that the ratio should be independent of t in the case of single-exponential decay. The non-single-exponential decay was noted also at 28 °C and 45 °C, as shown later in Figure 10. This behavior cannot be explained by the conventional molecular picture assuming the propagation only through the dissociated unimers (Scheme 1 and eq 3).

The conventional picture can be also tested for the t dependence of $\phi(t)$ observed for the polymerization batches of various initiator concentrations $[I]_0$. The conventional picture assumes that the propagation rate constant for the unimer k_1 and the f-mer/unimer equilibrium constant K_f depend on neither $[I]_0$ nor the concentration C and molecular weight M of the living polymer. Thus, this picture leads to a universal relationship between $\phi(t)$ and a normalized time t_n irrespective of the $[I]_0$ value (*cf.* eq 3),

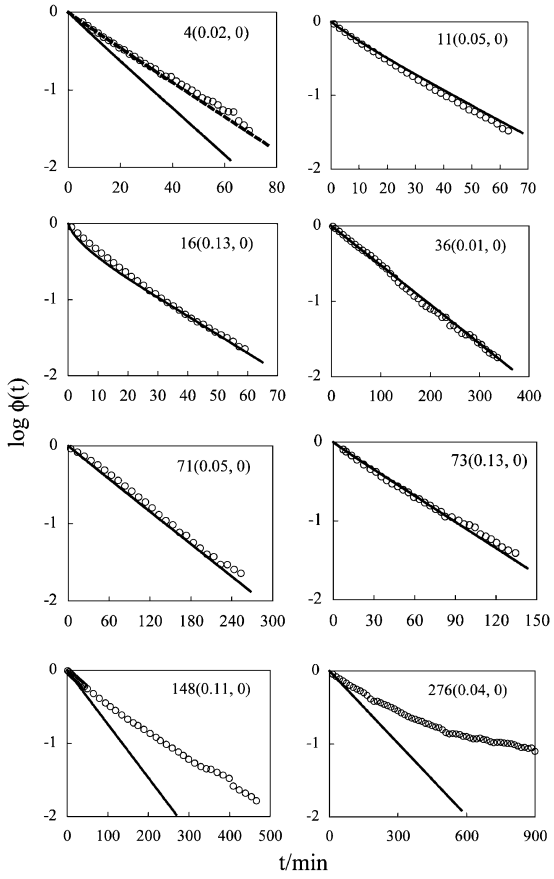

Figure 4. Decay of residual monomer fraction $\phi(t)$ during the polymerization process at 34.5 °C measured for the batches as indicated. These batches contained no dPS. Solid curves indicate $\phi(t)$ calculated from a kinetic model for a set of parameters $\tau' = 19\,\mathrm{min\,mol^{1/2}\,cm^{-3/2}}$, $A_2 = 1.8 \times 10^8\,\mathrm{mol^{-3/2}\,cm^{9/2}}$, and $A_3 = 2.1 \times 10^{15}\,\mathrm{mol^{-5/2}\,cm^{15/2}}$. Dotted curve for the lowest-M_{hPS} batch 4(0.02, 0) indicates the model calculation obtained by adjusting the propagation rate constant for the tetrameric aggregate (A_2) to zero. No adjustment was made for the other batches. For further details, see text.

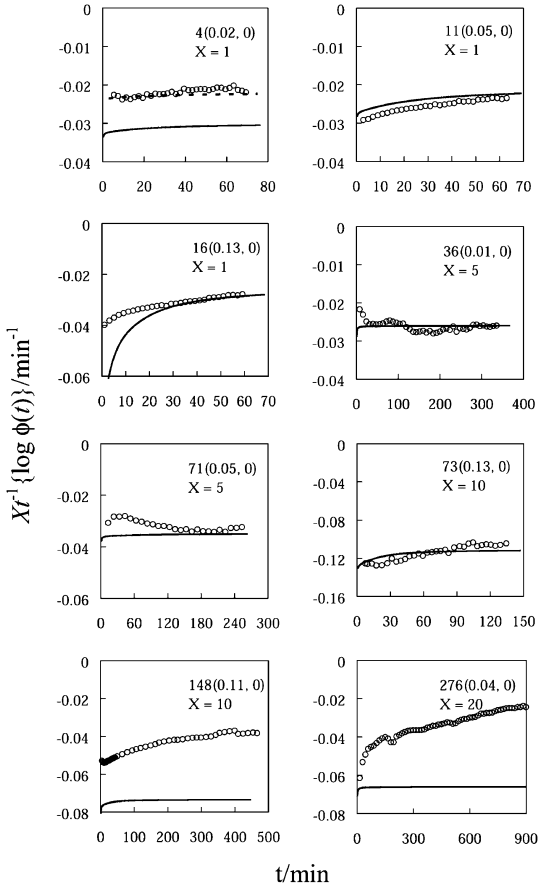

Figure 5. Plots of logarithm of residual monomer fraction reduced by time, $t^{-1}\{\log \phi(t)\}$, against the polymerization time t at 34.5 °C for the batches containing no dPS. The plots are vertically magnified by a factor X as indicated. Solid curves indicate $t^{-1}\{\log \phi(t)\}$ calculated from a kinetic model for a set of parameters $\tau' = 19\,\mathrm{min\,mol^{1/2}\,cm^{-3/2}}$, $A_2 = 1.8 \times 10^8\,\mathrm{mol^{-3/2}\,cm^{9/2}}$, and $A_3 = 2.1 \times 10^{15}\,\mathrm{mol^{-5/2}\,cm^{15/2}}$. For further details, see text.

$$\phi(t) = \exp(-k_1 K_f^{1/f} t_n) \quad \text{with} \quad t_n = \{[I]_0/f\}^{1/f} t \tag{5}$$

For hPSLi in a range of $10^{-3}M = 11$–160, the main aggregation number in cyclohexane at 35 °C is known to be $f = 2$.[1,12] Utilizing this f value and the $[I]_0$ data in Table I, we evaluated the normalized time t_n (eq 5) for the batches examined in Figures 4 and 5. Figure 6 shows plots of the $\log \phi(t)$ data for these batches against t_n. For the batches having $10^{-3}M_{\mathrm{hPS}}(\infty)$ in a rather narrow range between 4.2 and 73.2 (*cf.* Table I), the $\phi(t)$ data exhibit roughly universal t_n dependence, as similar to the behavior of hPBLi/Bz solutions examined previously.[25] However, this rough universality vanishes for higher $M_{\mathrm{hPS}}(\infty)$, as clearly seen for the batches 148(0.11, 0) and 276(0.04, 0). Thus, the conventional picture fails to explain the t dependence of the $\phi(t)$ data of the hPSLi/dCH solutions examined.

The above results are indicative of not only the failure of the conventional picture but also a more general feature of the polymerization of hPSLi in dCH, as noted from the following argument. In principle, the chemical equilibrium should hold between the unimers and all kinds of aggregates of various

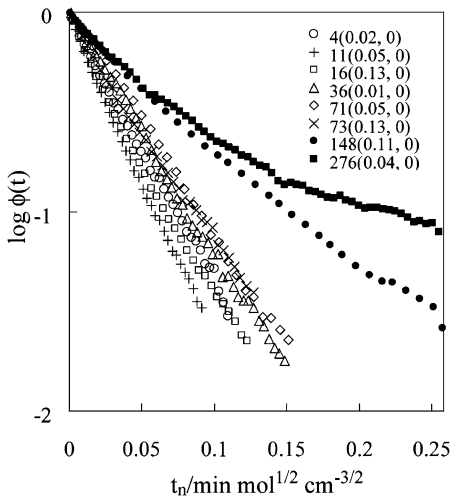

Figure 6. Residual monomer fraction $\phi(t)$ obtained at 34.5 °C for batches containing no dPB and having various $M_{\mathrm{hPS}}(\infty)$. The $\log \phi(t)$ data are plotted against normalized time, $t_n = t\{[I]_0/f\}^{1/f}$ with $f = 2$.

Polymer Journal

$$(\mathrm{PLi})_j \underset{}{\overset{K_j}{\rightleftharpoons}} j\mathrm{PLi} \quad (j = 2, 3, \ldots)$$

$$(\mathrm{PLi})_j + \mathrm{M} \xrightarrow[k_j]{} (\mathrm{PLi})_j \quad (j = 1, 2, 3, \ldots)$$

Scheme 2. General route of propagation through dissociated unimer and aggregates. $(\mathrm{PLi})_j$ with $j = 1$ stands for the unimer.

aggregation numbers j, although the equilibrium constant may be strongly dependent on j; see Scheme 2. Then, the monomer consumption rate during the propagation process can be written in a general form:

$$\frac{\mathrm{d[M]}}{\mathrm{d}t} = -\sum_{j\geq 1} k_j[\mathrm{P}_j][\mathrm{M}] \tag{6a}$$

with

$$[\mathrm{P}_j] = \frac{[\mathrm{P}_1]^j}{K_j} \tag{6b}$$

Here, k_j and $[\mathrm{P}_j]$ denote the propagation rate constant and molar concentration of the j-mer aggregate ($j \geq 1$; $j = 1$ stands for the dissociated unimer), and K_j represents the j-mer/unimer equilibrium constant with K_1 being defined as unity. Combining eq 6b with a mole conservation rule for all anionic species, $\Sigma_{j\geq 1} j[\mathrm{P}_j] = [\mathrm{I}]_0$, we find an equation that determines the unimer concentration $[\mathrm{P}_1]$,

$$\sum_{j\geq 1} \frac{j}{K_j}[\mathrm{P}_1]^j = [\mathrm{I}]_0 \tag{7}$$

This equation, if solved, should give $[\mathrm{P}_1]$ as a function of $[\mathrm{I}]_0$ and the equilibrium constants, *i.e.*, $[\mathrm{P}_1] = P_1([\mathrm{I}]_0; K_2, K_3, \ldots)$. Then, from eq 6b, eq 6a is rewritten as

$$\frac{\mathrm{d[M]}}{\mathrm{d}t} = -\lambda[\mathrm{M}] \text{ with } \lambda = \sum_{j\geq 1} \frac{k_j}{K_j}\{P_1([\mathrm{I}]_0; K_2, K_3 \ldots)\}^j \tag{8}$$

As noted from eq 8, $\phi(t)$ $(= [\mathrm{M}]/[\mathrm{M}]_0)$ always exhibits the *single-exponential* decay with the t-independent decay rate λ being determined by $[\mathrm{I}]_0$, K_j, and k_j, *given that* k_j and K_j $(j \geq 1)$ are determined only by the temperature and pressure irrespective of $[\mathrm{I}]_0$ and the molecular weight/concentration of the living polymer. Thus, the lack of the single-exponential behavior (Figure 4) suggests that k_j and K_j are dependent on either $[\mathrm{I}]_0$ or the polymer molecular weight/concentration, or both. This dependence is further discussed below in relation to the propagation behavior in the presence of the chemically inert dPS chains.

Propagation in Solutions in the Presence of dPS

Figure 7 compares t dependencies the $\phi(t)$ data of the polymerization batches 11(0.05, 0), 13(0.07, 0.09), and 17(0.09, 0.10) at 34.5 °C (*cf.* Table I). The last two batches contain dPS ($M_w = 56.8 \times 10^3$) at the concentrations above $C_{\mathrm{dPS}}{}^*$ $(= 0.066\,\mathrm{g\,cm^{-3}})$, while the first batch does not.

In general, the unimer molar concentration $[\mathrm{P}_1]$ increases with increasing $[\mathrm{I}]_0$ irrespective of the details of the propagation kinetics and chemical equilibrium. Eq 8 indicates that the $[\mathrm{I}]_0$ dependence of the decay rate λ emerges only through

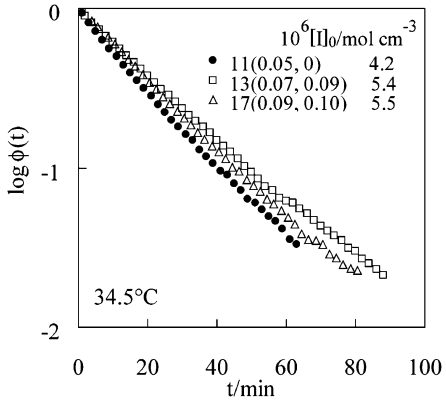

Figure 7. Comparison of residual monomer fraction $\phi(t)$ at 34.5 °C measured for batches 11(0.05,0), 13(0.07,0.09), and 17(0.09,0.10) having roughly the same $M_{\mathrm{hPS}}(\infty)$. The initiator concentration $[\mathrm{I}]_0$ increases in this order. The batch 11(0.05,0) contained no dPS, while the other two batches contained semi-dilute dPS.

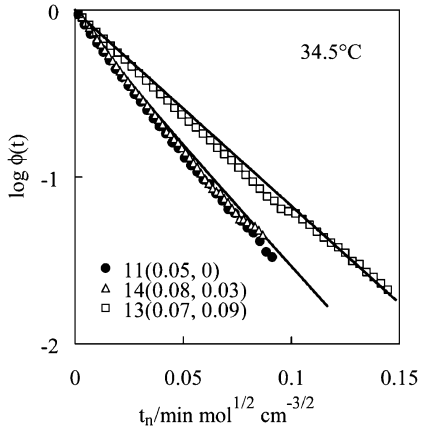

Figure 8. Comparison of residual monomer fraction $\phi(t)$ for the batches 11(0.05,0), 14(0.08,0.03), and 13(0.07,0.09) having nearly the same $M_{\mathrm{hPS}}(\infty)$ but different C_{dPS}. The $\log\phi(t)$ data are plotted against normalized time, $t_n = t\{[\mathrm{I}]_0/f\}^{1/f}$ with $f = 2$. Solid curves indicate $\phi(t)$ calculated from a kinetic model described in the text.

$P_1([\mathrm{I}]_0; K_2, K_3, \ldots)$ if *none* of the propagation rate constants k_j and the equilibrium constants K_j is dependent on $[\mathrm{I}]_0$ and polymer concentration/molecular weight. For this case, the increase of $[\mathrm{I}]_0$ (always enlarging $[\mathrm{P}_1]$) leads to an increase of λ (= given by a sum of power-law series of $[\mathrm{P}_1]$; *cf.* eq 8), *i.e.*, to the accelerated decay of $\phi(t)$. Nevertheless, Figure 7 demonstrates that the decay of $\phi(t)$ was slower for the batches 13(0.07, 0.09) and 17(0.09, 0.10) than for the batch 11(0.05, 0), with the former two having larger $[\mathrm{I}]_0$ than the latter. This result unequivocally indicates that some of k_j and K_j are affected by the dPS chains not chemically involved in the propagation reaction.

As a further test of this effect of chemically inert dPS, Figures 8 and 9 examine the $\phi(t)$ data at 34.5 °C obtained for the batches having nearly the same hPS molecular weight $M_{\mathrm{hPS}}(\infty)$ on completion of polymerization but different dPS concentrations C_{dPS}. The curves indicate the results of calculation with a kinetic model explained later. Since these batches had different $[\mathrm{I}]_0$ (*cf.* Table I), a direct comparison of

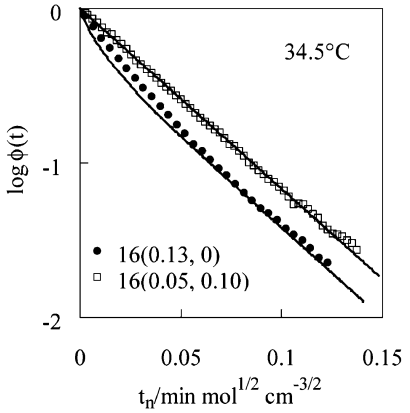

Figure 9. Comparison of residual monomer fraction $\phi(t)$ for the batches 16(0.13,0) and 16(0.05,0.10) having almost identical $M_{hPS}(\infty)$ but different C_{dPS}. The $\log \phi(t)$ data are plotted against normalized time, $t_n = t\{[I]_0/f\}^{1/f}$ with $f = 2$. Solid curves indicate $\phi(t)$ calculated from a kinetic model described in the text.

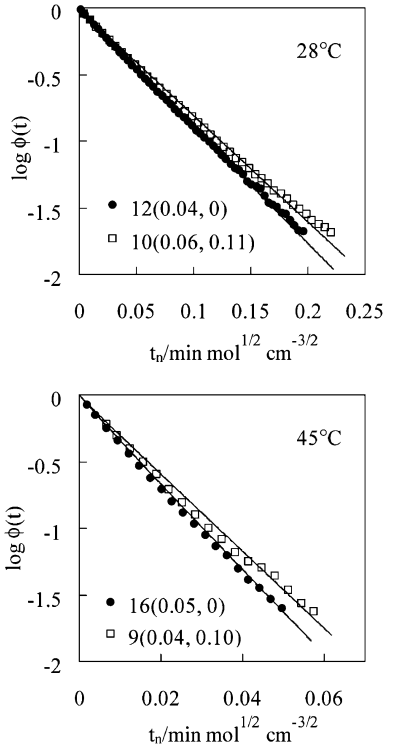

Figure 10. Comparison of residual monomer fraction $\phi(t)$ measured for batches 12(0.04,0), 10(0.06,0.11) at 28.0 °C (top panel) and for batches 16(0.05,0) and 9(0.04,0.10) at 45.0 °C (bottom panel). The $\log \phi(t)$ data are plotted against normalized time, $t_n = t\{[I]_0/f\}^{1/f}$ with $f = 2$. In each panel, the two batches with/without dPS had roughly the same $M_{hPS}(\infty)$.

the $\log \phi(t)$ *vs* t plots did not give a clear insight for the effect of dPS. Thus, on the basis of the rough universality of the dependence of $\phi(t)$ on t_n ($= t\{[I]_0/f\}^{1/f}$ with $f = 2$) seen in the range of $10^{-3}M_{hPS}(\infty) = 4.2$–$73.2$ (Figure 6), Figure 8 compares the $\log \phi(t)$ *vs* t_n plots for the batches 11(0.05,0), 14(0.08, 0.03), and 13(0.07,0.09) having nearly the same $M_{hPS}(\infty)$ in this range: *cf.* Table I. Similarly, Figure 9 compares the $\log \phi(t)$ *vs* t_n plots for the batches 16(0.13,0) and 16(0.05,0.10) having almost identical $M_{hPS}(\infty)$. The batches 13(0.07,0.09) and 16(0.05,0.10) have $C_{dPS} > C_{dPS}^*$ ($= 0.066\,g\,cm^{-3}$), while the batch 14(0.08, 0.03) has $C_{dPS} < C_{dPS}^*$. We note that dilute dPS in the batch 14(0.08, 0.03) hardly affects the decay of $\phi(t)$ with t_n (*cf.* Figure 8) while semi-dilute dPS in the batches 13(0.07,0.09) and 16(0.05,0.10) considerably retards this decay (*cf.* Figures 8 and 9).

This slowing due to semi-dilute dPS was noted also at 28 °C and 45 °C, as shown in Figure 10 where the $\log \phi(t)$ *vs* t_n plots at these temperatures are compared for the batches having roughly the same $10^{-3}M_{hPS}(\infty)$ but different C_{dPS}. The magnitude of slowing (compared to the batches without dPS) is similar at temperatures between 28 °C and 45 °C, as noted for the plots for the batches 10(0.06,0.11), 16(0.05,0.10) and 9(0.04,0.10) having nearly the same C_{dPS} ($\cong 0.10\,g\,cm^{-3}$) and being examined at 28.0, 34.5, and 45.0 °C, respectively; *cf.* Figures 9 and 10.

Osmotic Effect on Aggregate Fusion

The slowing of the propagation due to semi-dilute dPS chains (Figures 8–10) is similar to that seen for the hPBLi/dPB/Bz systems.[25] This slowing can be related, in principle, to several effects of the dPS chains on the hPSLi anions, (1) a change in the polarity in the system that may affect the anion reactivity, (2) a decrease of the mobility of the hPSLi unimers/aggregates, (3) shift of the equilibrium between the unimers and aggregates (mainly dimers) toward the latter, and (4) an enhancement of the osmotic barrier for the fusion of the aggregates, as discussed previously.[25] The effect (1) should be irresponsible for the observed slowing because dPS and the solvent, dCH, are almost equally nonpolar. The effect (2) would be also minor because the unimers and dimeric aggregates coexisting with dPS during the propagation examined in Figures 7–10 were of just low molecular weights ($M < 2M_{hPS}(\infty) \leq 34.6 \times 10^3$; *cf.* Table I). The mobilities of such low-M unimers/dimers would not be significantly affected by the semi-dilute dPS chains, in particular in the early state of propagation.

As for the effect (3), an anonymous reviewer for this paper suggested that the equilibrium constant K_2 (eq 2) for the unimer and dimer (having molecular weights M and $2M$ and the total concentration C) may be approximately expressed as $K_2 \propto \exp\{(\mu_2^\circ - 2\mu_1^\circ)/RT - 2M(a_{11} - a_{22})C - M(a_{111} - a_{222})C^2\}$ up to the third virile expansion. Here, μ_i° is the standard chemical potential and a_{ii} and a_{iii} are the second and third virial coefficients defined for the unimer ($i = 1$) and dimer ($i = 2$), respectively, R is the gas constant, and T is absolute temperature. If $2(a_{11} - a_{22}) + (a_{111} - a_{222})C > 0$, this K_2 decreases with increasing C and M and the corresponding enrichment of dimer (= decrease of the unimer concentration) could, *in principle*, result in the slowing of propagation due to dPS as well as the non-exponential decay of $\phi(t)$ during the propagation in the absence of dPS. However, the values of a_{ii} and a_{iii} determined by the interaction among unimers/dimers are unknown for the anionic hPSLi unimer and $(hPSLi)_2$ dimer

($a_{ii} = 0$ for high-M, *neutral* hPS in cyclohexane at 34.5 °C, but this is not the case for our unimer/dimer), and the above expression of K_2 *does not* straightforwardly indicates that the enrichment of dimer (effect (3)) is the main factor leading to the slowing of propagation due to dPS (and the non-exponential propagation behavior in the absence of dPS).

Concerning this point, the $\phi(t)$ data of the batches 14(0.08,0.03) and 11(0.05,0) with and without dPS (*cf.* Figure 8) provide us with a clue for specifying the mechanism of slowing. The total polymer concentration C in the batch 11(0.05,0) remains smaller than $0.025\,\mathrm{g\,cm^{-3}}$ in a range of $\phi(t) > 0.46$, suggesting that the interaction determining a_{ii} and a_{iii} in this batch at $\phi(t) > 0.46$ is weaker than that in the batch 14(0.08,0.03) having $C_{\mathrm{dPS}} = 0.025\,\mathrm{g\,cm^{-3}}$ and $C \geq 0.025\,\mathrm{g\,cm^{-3}}$ at any $\phi(t)$. Thus, *if* the observed slowing is mainly due to the enrichment of dimer, the slowing should be more significant, at least in the range of $\phi(t) > 0.46$, for 14(0.08,0.03) than for 11(0.05,0), the former having larger C and M_{hPS} than the latter at any given value of $\phi(t)$. Nevertheless, the two batches 14(0.08,0.03) and 11(0.05,0) exhibit indistinguishable decay of $\phi(t)$ with the normalized time t_{n} not only at $t_{\mathrm{n}} < 0.018\,\mathrm{min\,mol^{1/2}\,cm^{-3/2}}$ (where $\phi(t) > 0.46$ for both batches) but also at longer t_{n}; see Figure 8. Furthermore, the slowing should become less significant at higher T (where the dissociation is enhanced) *if* the slowing is mainly due to the enrichment of dimer, but the magnitude of slowing is similar at T between 28.0 °C and 45.0 °C as explained earlier for Figures 9 and 10. These facts strongly suggests that the enrichment of the dimer is not the main factor responsible for the slowing of propagation due to dPS (as well as the non-exponential propagation behavior in the absence of dPS) in the batches examined in this study, although the enrichment may have occurred to some extent to give a secondary effect on the propagation.

Thus, the slowing of the hPSLi propagation due to dPS seems to be mainly due to the effect (4), the enhancement of the osmotic barrier for the fusion of the most stable aggregates (hPSLi dimers) into larger aggregates. This barrier can be examined through the ^{7}Li NMR spectra that reflect the Li-Li exchange of these aggregates. As an example, Figure 11 shows the spectra measured at 34.5 °C for the batches 11(0.05,0), 16(0.13,0), and 16(0.05,0.10) after completion of polymerization. The integrated intensity of the spectra is normalized to unity. Only the batch 16(0.05,0.10) contained semi-dilute dPS. All batches exhibit multiple peaks at the chemical shifts $\delta \cong 0.2$, -0.8, -2.1, and -4.0 ppm (relative to LiCl in D_2O), although the two low-δ peaks are weak in the batches 11(0.05,0), 16(0.13,0). The multiple peaks unequivocally indicate that the Li in the hPSLi/dPS/CH solutions is in several aggregation states and the exchange of these Li species is slow compared to the NMR time scale:[22,31] Note that a single peak is to be observed if the exchange is sufficiently fast, as discussed previously for mono-anionic PBLi and bi-anionic $PBLi_2$ chains in deuterated benzene.[22,31]

It is informative to compare the behavior of our the hPSLi chains with that of the PBLi and $PBLi_2$ chains. For the mono-anionic PBLi chains, the multiple peaks, seen at low temperatures T, changed into a single peak at high T, and the chemical shift δ of the single peak at high T was between those of the multiple peaks at low T.[22] This change is attributed to acceleration of exchange of Li species in *homogeneous* systems. In contrast, for the bi-anionic $PBLi_2$, one of the multiple peaks at low T increased its intensity with increasing T while the other peaks decreased their intensities and these changes were associated with no change in the δ values of the peaks.[31] This behavior is attributable to enhanced exchange of Li species that are in *inhomogeneous* states[32] and have the lifetime distribution, as discussed previously.[31] For our hPSLi systems (Figure 11), we note that the intensities of the lowest-δ peak and higher-δ peaks are considerably larger and smaller, respectively, for the batches 11(0.05,0), 16(0.13,0) than for the batch 16(0.05,0.10) while all these batches have common δ values of the peaks. This feature is qualitatively similar to that observed for the bi-anionic $PBLi_2$ chains on an increase of T, with the low-T behavior of $PBLi_2$ corresponding to the behavior of the batch 16(0.05,0.10). This similarity suggests that the exchange of Li species of hPSLi (possibly in the inhomogeneous states) is slower in the batch 16(0.05,0.10) containing semi-dilute dPS than in the batches 11(0.05,0) and 16(0.13,0) without dPS, despite a fact that 16(0.05,0.10) and 16(0.13,0) have almost identical $M_{\mathrm{hPS}}(\infty)$ and nearly the

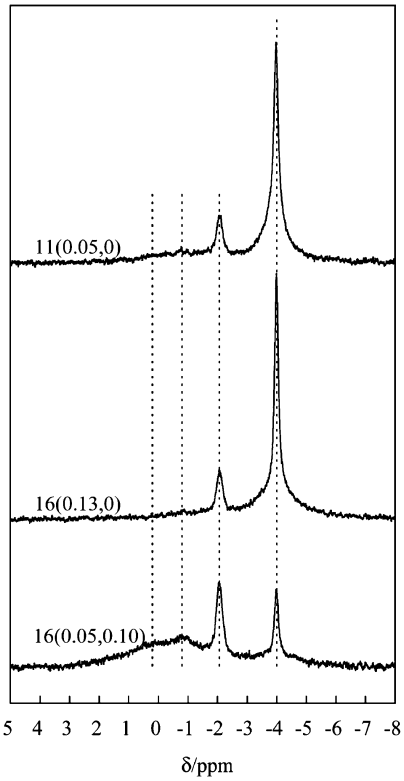

Figure 11. ^{7}Li NMR spectra of batches 11(0.05,0), 16(0.13,0), and 16(0.05,0.10) after completion of polymerization. The spectra were measured at 34.5 °C, and their intensities were normalized to unity. The three batches had nearly the same $M_{\mathrm{hPS}}(\infty)$, and the latter two batches contained semi-dilute dPS.

same total polymer concentration (hPSLi plus dPS) while 16(0.05,0.10) and 11(0.05,0) have roughly the same $M_{hPS}(\infty)$ and $C_{hPS}(\infty)$; *cf.* Table I.

In general, the Li-Li exchange is slower when an average distance d between hPSLi aggregates is larger and their thermal mobility μ is smaller.[22] However, the above comparison of the three batches suggests that the exchange in 16(0.05,0.10) is considerably slower than expected from this general behavior. (Note that d is nearly the same for the batches 16(0.05,0.10) and 11(0.05,0) and that μ of the low-M hPSLi chains should not be significantly affected by dPS in particular in the early stage of propagation.) This extra slowing in the batch 16(0.05,0.10) possibly reflects an osmotic barrier for the hPSLi dimer fusion due to the semi-dilute dPS chains, as similar to the situation seen for hPBLi/dPB/Bz systems.[25]

Kinetic Model for Unimer/aggregates Systems

The above results lead to a hypothesis that large aggregates resulting from fusion of the linear dimers of hPSLi (most stable aggregates) has an important contribution to the propagation in the absence of dPS and the osmotic barrier due to dPS suppresses this fusion and thus retards the propagation. This hypothesis is tested below through a simple kinetic model.

In general, the most stable aggregate would be in equilibrium with aggregates of various, finite sizes (with the equilibrium constants changing with the aggregation number), as suggested from a static/dynamic light scattering experiment.[21] Thus, for our PSLi anionic systems, we may safely assume that the unimer and all aggregates, being at equilibrium, are reactive with the monomers *except* the most stable dimeric aggregates, as shown in Scheme 3. (Partly following the conventional molecular picture (Scheme 1), we have assumed that the most stable dimer is well stabilized through its Li-Li bond and thus not reactive.) Specifically, Scheme 3 considers only $2n$-mer aggregates ($n \geq 2$) formed through fusion of n dimers because the aggregates having odd aggregation numbers, formed through fusion of the dimers and unimers, should be much more dilute even compared to the dilute unimers. (Scattering/viscosity data for PSLi chains indicate that the unimers are dilute in the systems.[1–4,12]) The equilibrium constant between the dimer and $2n$-mer aggregates, K'_n, is defined by

$$K'_n = \frac{[P_{2n}]}{[P_2]^n} \cong \frac{[P_{2n}]}{\{[I]_0/2\}^n} \tag{9}$$

$$(PLi)_2 \underset{}{\overset{K_2}{\rightleftharpoons}} 2PLi$$

$$n(PLi)_2 \overset{K'_n}{\rightleftharpoons} (PLi)_{2n} \quad (n = 2, 3, \ldots)$$

$$PLi + M \xrightarrow[k_1]{} PLi$$

$$(PLi)_{2n} + M \xrightarrow[k_{2n}]{} (PLi)_{2n} \quad (n = 2, 3, \ldots)$$

Scheme 3. Propagation through dissociated unimer and fused $2n$-mer aggregates ($n \geq 2$).

with $[P_{2n}]$ being the molar concentration of the $2n$-mer; *cf.* Scheme 3. Since the dimer is the dominant component in the system, we approximate its concentration as $[P_2] \cong [I]_0/2$ and thus $[P_{2n}] \cong K'_n\{[I]_0/2\}^n$; *cf.* eq 9. The equilibrium constant between the dimer and unimer is identical to that defined by eq 2 (with $f = 2$), and the unimer concentration is approximated as $[P_1] \cong \{K_2[I]_0/2\}^{1/2}$. The propagation rate constants for the $2n$-mer and unimer, identical to those define by eq 6a, are denoted by k_{2n} and k_1, respectively.

The kinetic equation corresponding to Scheme 3 is written as

$$\frac{d\{\ln \phi(t)\}}{dt} = -k_1[P_1] - \sum_{n\geq 2} k_{2n}[P_{2n}]$$

$$\cong -\frac{[I]_0^{1/2}}{\tau'} - \sum_{n\geq 2} k_{2n}K'_n\{[I]_0/2\}^n$$

$$\text{with } \tau' = \frac{1}{k_1}\left(\frac{2}{K_2}\right)^{1/2} \tag{10}$$

The equilibrium constant for the $2n$-mer, K'_n, may be expressed as a product of a non-osmotic contribution K''_n and an osmotic contribution, $\exp(-\Delta G_{os}^{[n]}(t)/k_BT)$, as discussed previously.[25] Here, $\Delta G_{os}^{[n]}$ is the osmotic free energy increment on fusion of n dimers into a $2n$-mer, k_B is the Boltzmann constant, and T is the absolute temperature. After this factorization of $\Delta G_{os}^{[n]}$, eq 10 becomes

$$\frac{d\{\ln \phi(t)\}}{dt} = -\frac{[I]_0^{1/2}}{\tau'}\left[1 + \sum_{n\geq 2} A_n [I]_0^{n-1/2} \exp\left(-\frac{\Delta G_{os}^{[n]}(t)}{k_BT}\right)\right] \tag{11}$$

with A_n being a normalized propagation rate constant for the $2n$-mer defined by

$$A_n = \frac{k_{2n}K''_n}{2^{n-1/2}k_1K_2^{1/2}} \tag{12}$$

In what follows, we first express $\Delta G_{os}^{[n]}$ in terms of local concentrations and then test our kinetic model, eq 11, on the basis of this expression.

Expression of the Osmotic Free Energy Increment $\Delta G_{os}^{[n]}(t)$

We formulate $\Delta G_{os}^{[n]}$ appearing in eq 11 in a way similar to that in the previous work[25] but with a small improvement (through consideration of the fused $2n$-mer with $n \geq 2$ and treatment of background concentration explained later). Figure 12 illustrates the geometry for this formulation. The dPS chains, when existing, are considered to have a concentration $C_{dPS} > C_{dPS}^*$ thereby suppressing osmotically the fusion of hPSLi dimers into a larger aggregate. $\Delta G_{os}^{[n]}$ increases whenever a dimer and other aggregate approach each other and enhance their mutual overlapping. The tetramer is formed through an approach of a dimer toward the other dimer; *cf.* upper part of Figure 12. A larger $2n$-mer ($n \geq 3$) is considered to be formed through an approach of $2(n-1)$-mer toward a dimer; for example a hexamer is formed through an approach of a tetramer toward a dimer; *cf.* lower part of Figure 12. This

Polymer Journal

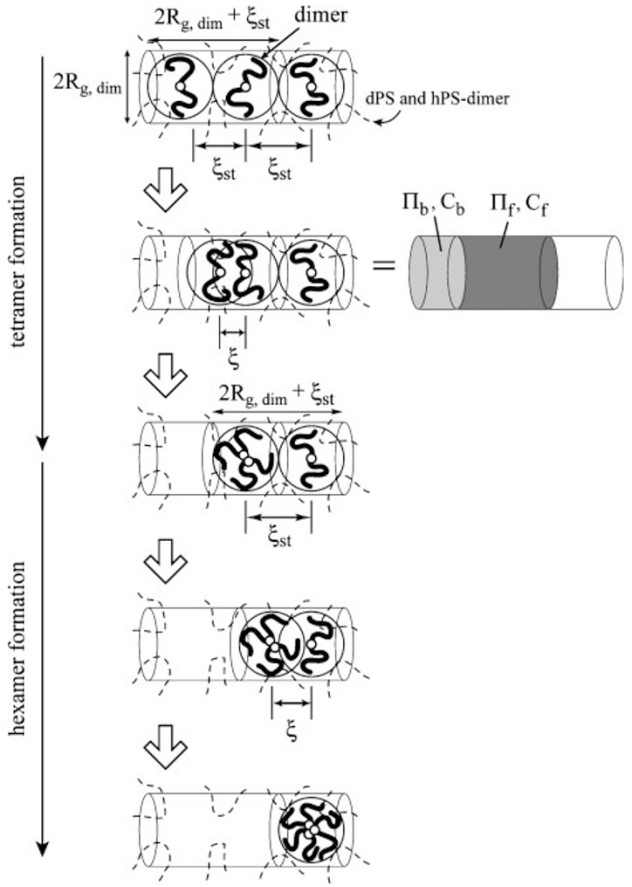

Figure 12. Schematic illustration of a geometry considered for calculation of the osmotic free energy increment on fusion of hPSLi dimers into tetramer and hexamer.

does not mean that the $2(n-1)$-mer moves faster than the smaller dimer. Instead, the $2(n-1)$-mer aggregate is slowly pushed toward the dimer in order to calculate $\Delta G_{os}^{[n]}$ in a stepwise way.

The center-to-center distance of two dimers at the onset of enhancement of their mutual overlapping, ξ_{st}, is chosen to be[25]

$$\text{for } C_{hPS} < C_{dim}^*\text{: } \xi_{st} = 2R_{g,dim} \tag{13a}$$

$$\text{for } C_{hPS} > C_{dim}^*\text{: } \xi_{st} = 2(3/4\pi)^{1/3}\{2M/N_A C_{hPS}\}^{1/3} = 2R_{g,dim}(C_{dim}^*/C_{hPS})^{1/3} \tag{13b}$$

Here, C_{hPS} is the total concentration of hPSLi chains ($\cong$ dimer concentration), C_{dim}^* is the overlapping concentration of the dimer having the radium of gyration $R_{g,dim}$, M is the unimer molecular weight, and N_A is the Avogadro constant. These choices are based on the following simple argument: If $C_{hPS} < C_{dim}^*$, the dimers are dilute and the osmotic free energy begins to increase significantly only after two dimers come to the touching location at $\xi_{st} = 2R_{g,dimer}$ (eq 13a). On the other hand, for $C_{hPS} > C_{dim}^*$, an approach of the dimers by any distance enhances the overlapping to give this increase. For this case, ξ_{st} is essentially identical to the equilibrium center-to-center separation of the two dimers, $\sim \{2M/N_A C_{hPS}\}^{1/3}$. The front factor of $2(3/4\pi)^{1/3}$ ($\cong 1.24$) has been introduced in eq 13b in order to ensure the continuity of ξ_{st} at $C_{hPS} = C_{dim}^*$.

For the approach of the $2(n-1)$-mer aggregate toward the dimer (*i.e.*, for the $2n$-mer formation), the mutual overlapping begins to be enhanced at the same ξ_{st} as defined above, as can be noted from the lower part of Figure 12. (Strictly speaking, R_g increases a little with increasing n. However, we neglect this increase for simplicity.) Thus, we utilize eq 13a and 13b also for the case of the $2n$-mer formation with $n \geq 3$.

$\Delta G_{os}^{[n]}$ can be expressed in terms of the osmotic pressures Π_f and Π_b in the forward and backward regimes shown in Figure 12:[25]

$$\Delta G_{os}^{[n]} = \sum_{m=2}^{n} g_{os}^{[m]} \quad \text{with} \quad g_{os}^{[m]} = -\pi R_{g,dim}^2 \int_{\xi_{st}}^{0} \{\Pi_f - \Pi_b\} d\xi \tag{14}$$

Here, the front factor $\pi R_{g,dim}^2$ represents the cross-sectional area of those regimes, ξ is the center-to-center distance of the approaching aggregates, and ξ_{st} (eq 13) is the distance at the onset of $\Delta G_{os}^{[n]}$ increase. As explained for Figure 12, the $2n$-mer formation with $n \geq 3$ is considered to occur in a stepwise way, *i.e.*, the formation of tetramer, the formation of hexamer *via* the approach of tetramer toward dimer, ..., occurring in this order. The factor $g_{os}^{[m]}$ appearing in eq 14 represents the osmotic free energy increment for each step.

For neutral, high-M linear hPS, the osmotic pressure Π is expressed in the standard, semi-dilute scaling form.[26,33,34] Specifically, an empirical equation describing both of the scaling exponent and numerical prefactor of the Π data has been reported for hPS/CH solutions at 34.5 °C.[26] (The prefactor is very close to unity for hPS/CH.[26]) The thermodynamic states of the anionic $(hPSLi)_{2n}$ aggregates ($n = 1, 2, \ldots$) in dCH would be somewhat different from those of the corresponding, neutral hPS chains, as explained earlier in relation to the unimer/dimer equilibrium constant. However, because of the absence of the Π data for the aggregates, we utilize the empirical equation for the high-M neutral hPS for simplicity to describe Π_f and Π_b of the aggregates in terms of the polymer concentrations C_f and C_b in the forward and backward regimes and the overlapping concentration of the dimer, C_{dim}^*:

$$\Pi_\alpha = \frac{C_\alpha RT}{2M}\left(\frac{C_\alpha}{C_{dim}^*}\right)^2 \quad \text{for hPS/dCH } (\alpha = \text{f, b}) \tag{15}$$

Here, R and T are the gas constant and absolute temperature, respectively, and M is the unimer molecular weight. In eq 15, the concentration C_α is scaled with C_{dim}^* so that the dimer molecular weight $2M$ is included therein.[25] The concentrations C_b and C_f included in eq 15 is expressed in terms of the center-to-center distance ξ of the approaching aggregates, as explained below.

Expression of Concentrations in Backward and Forward Regimes

The concentrations C_f and C_b in the forward and backward regimes (*cf.* Figure 12) are different from the average concentration of the polymers (dPB plus hPB) in the system, $C_{dPB} + C_{hPS}(t)$. The ξ dependencies of C_f and C_b can be found

from a simple geometrical analysis incorporating a background concentration, as discussed below.

For the tetramer formation (dimer-dimer fusion) in the dilute limit of $C_{hPS} \to 0$, the combined forward plus backward regime contains only two hPSLi dimers (plus dPS chains being distributed uniformly in the system). Then, C_b in the backward regime is simply given by the dPS concentration C_{dPS} ($> C_{dPS}{}^*$), as considered previously.[25] However, at non-zero C_{hPS} (still smaller than $C_{dim}{}^*$), the combined regime should contain more than two dimers because the random coils of the two dimers each having the volume $4\pi R_{g,dim}^3/3$ do not fully occupy the combined regime having the volume $4\pi R_{g,dim}^3$ at the dimer-dimer contact ($\xi = \xi_{st}$; *cf.* eq 13a). Thus, we consider that the hPSLi chains (mainly dimers) in the system visit the unoccupied region (of the volume $4\pi R_{g,dim}^3/3$) at equilibrium to provide this region with the average concentration, C_{hPS}. During the fusion process, the mass supplied by those hPSLi chains, $4\pi C_{hPS} R_{g,dim}^3/3$, is assumed to be uniformly distributed in the combined regime of volume $4\pi R_{g,dim}^3$ to give the background hPS concentration, $C_{hPS}/3$. Then, the total polymer concentration in the backward regime (= total background concentration of hPS and dPS) is estimated to be

$$C_b = C_{dPS} + \frac{C_{hPS}}{3} \quad \text{(for tetramer formation at } C_{hPS} < C_{dim}{}^*\text{)} \tag{16a}$$

This C_b is considered to remain constant during the fusion process.

The concentration C_f in the forward regime during this process can be evaluated on the basis of the mass conservation. The backward and forward regimes have the volumes $\pi R_{g,dim}^2(\xi_{st} - \xi)$ $(= \pi R_{g,dim}^2(2R_{g,dim} - \xi)$; *cf.* eq 13a and $\pi R_{g,dim}^2(2R_{g,dim} + \xi)$, respectively; see upper part of Figure 12. The corresponding masses in these regimes are $\pi C_b R_{g,dim}^2(2R_{g,dim} - \xi)$ and $\pi C_f R_{g,dim}^2(2R_{g,dim} + \xi)$. The polymer mass in the combined backward plus forward regime is given by $4\pi C_b R_{g,dim}^3 + 4M/N_A$, where $4\pi C_b R_{g,dim}^3$ is the contribution from the total background concentration and $4M/N_A$ is the mass of two dimers approaching each other (M = unimer molecular weight). Thus, the mass conservation leads to

$$C_f = C_b + \frac{8R_{g,dim}}{3(2R_{g,dim} + \xi)} C_{dim}{}^* \quad \text{(for tetramer formation at } C_{hPS} < C_{dim}{}^*\text{)} \tag{16b}$$

(In derivation of eq 16b, we have utilized a relationship, $C_{dim}{}^* = \{2M/N_A\}/\{4\pi R_{g,dim}^3/3\}$.)

For the tetramer formation of semi-dilute dimers having $C_{hPS} > C_{dim}{}^*$, the concentrations in the backward and forward regimes can be similarly estimated by considering the background concentration. The total hPS mass in the combined regime at the onset of the increase of $\Delta G_{os}^{[n]}$ is written as $\pi C_{hPS} R_{g,dim}^2(2R_{g,dim} + \xi_{st})$ with ξ_{st} being given by eq 13b. The background hPS mass is obtained by subtracting the mass of two approaching dimers, $4M/N_A$, from the total hPS mass. Thus, the total background concentration of hPS and dPS is estimated to be

$$C_b = C_{dPS} + C_{hPS} - \frac{(4M/N_A)}{\pi R_{g,dim}^2(2R_{g,dim} + \xi_{st})} = C_{dPS} + C_{hPS} - \frac{8R_{g,dim}}{3(2R_{g,dim} + \xi_{st})} C_{dim}{}^* \quad \text{(for tetramer formation at } C_{hPS} > C_{dim}{}^*\text{)} \tag{17a}$$

From the mass conservation requirement, $\pi C_b R_{g,dim}^2(\xi_{st} - \xi) + \pi C_f R_{g,dim}^2(2R_{g,dim} + \xi) = 4\pi C_b R_{g,dim}^3 + 4M/N_A$, the concentration in the forward regime C_f is obtained as

$$C_f = \left(1 + \frac{2R_{g,dim} - \xi_{st}}{2R_{g,dim} + \xi}\right) C_b + \frac{8R_{g,dim}}{3(2R_{g,dim} + \xi)} C_{dim}{}^* \quad \text{(for tetramer formation at } C_{hPS} > C_{dim}{}^*\text{)} \tag{17b}$$

For the approach of the $2(n-1)$-mer aggregate with $n \geq 3$ toward the dimer (*i.e.*, for the $2n$-mer formation; *cf.* lower part of Figure 12), the concentrations in the forward and backward regimes can be similarly estimated. The total background concentration of dPS and hPS is considered to be identical to that evaluated for the tetramer formation (eqs 16a and 17a), while the total mass of the two approaching aggregates (dimer and $(2(n-1)$-mer), $2nM/N_A$ with $n \geq 3$, is larger than that for the tetramer formation ($= 4M/N_A$). Considering this point, we find an expression of C_f for the $2n$-mer formation:

$$C_f = C_b + \frac{4nR_{g,dim}}{3(2R_{g,dim} + \xi)} C_{dim}{}^* \quad \text{(for } 2n\text{-mer formation at } C_{hPS} > C_{dim}{}^*\text{)} \tag{18}$$

and

$$C_f = \left(1 + \frac{2R_{g,dim} - \xi_{st}}{2R_{g,dim} + \xi}\right) C_b + \frac{4nR_{g,dim}}{3(2R_{g,dim} + \xi)} C_{dim}{}^* \quad \text{(for tetramer formation at } C_{hPS} < C_{dim}{}^*\text{)} \tag{19}$$

Test of Kinetic Model

Utilizing eqs 15–19, we can analytically conduct the integrals for $g_{os}^{[m]}$ appearing in eq 14: $g_{os}^{[2]}$ for the tetramer formation is calculated by using C_b and C_f given by eqs 16 and 17. For the calculation of $g_{os}^{[m]}$ ($m \geq 3$), the expression of C_f is changed to that given by eqs 18 and 19 with $n = m$. The results for any m value can be summarized as

$$\frac{g_{os}^{[m]}}{k_B T} = \{3\ln 2\} m \left(\frac{C_b}{C_{dim}{}^*}\right)^2 + m^2 \left(\frac{C_b}{C_{dim}{}^*}\right) + \frac{m^3}{6} \quad \text{for } C_{hPS} < C_{dim}{}^* \ (m = 2, 3, 4, \ldots) \tag{20}$$

$$\frac{g_{os}^{[m]}}{k_B T} = \frac{9}{2}\left(\frac{C_b}{C_{dim}{}^*}\right)^2 \left\{\left(\frac{C_b}{C_{dim}{}^*}\right)(1-r) + \frac{2m}{3}\right\} \ln(1+r) + \frac{9}{2}\left(\frac{C_b}{C_{dim}{}^*}\right)\left\{\left(\frac{C_b}{C_{dim}{}^*}\right)(1-r) + \frac{2m}{3}\right\}^2 \left\{1 - \frac{1}{1+r}\right\} + \frac{3}{4}\left\{\left(\frac{C_b}{C_{dim}{}^*}\right)(1-r) + \frac{2m}{3}\right\}^3 \left\{1 - \frac{1}{(1+r)^2}\right\} \quad \text{for } C_{hPS} > C_{dim}{}^* \ (m = 2, 3, 4, \ldots) \tag{21a}$$

with

$$r = \left(\frac{C_{dim}{}^*}{C_{hPS}}\right)^{1/3} \tag{21b}$$

The C_b appearing in eqs 20 and 21 are given by eqs 16a and 17a. (The functional form of these $g_{os}^{[m]}$ is different from that of $\Delta G_{os}^{[2]}$ derived previously without considering the background concentration. However, a numerical difference was not very large.)

Substituting eqs 20 and 21 in eq 14, we obtain an explicit expression of the free energy increment for the $2n$-mer formation, $\Delta G_{os}^{[n]}$, in terms of C_{dPS}, C_{hPS}, and the unimer molecular weight M that determines $C_{dim}{}^*$ through a relationship $C_{dim}{}^* = \{2M/N_A\}/\{4\pi R_{g,dim}^3/3\}$. Note that $R_{g,dim}$ of the dimer, evaluated from an empirical equation[30] ($R_{g,dim} = 3.0 \times 10^{-9} \times (2M)^{1/2}$ cm for hPS/CH at 34.5 °C), is determined only by M.

The time evolution for the residual hS monomer fraction $\phi(t)$, eq 11, can be solved with this explicit expression of $\Delta G_{os}^{[n]}$. However, we should note that both of the unimer molecular weight M and the total hPS concentration C_{hPS} increase with t during the propagation process and are related to $\phi(t)$ as

$$M(t) = \{M_{hPS}(\infty) - M_{oS}\}\{1 - \phi(t)\} + M_{oS} \quad (22a)$$

$$C_{hPS}(t) = C_{hPS}(\infty)\left\{1 - \frac{M_{oS}}{M_{hPS}(\infty)}\right\}\{1 - \phi(t)\} + C_{hPS}(\infty)\frac{M_{oS}}{M_{hPS}(\infty)} \quad (22b)$$

Here, M_{oS} ($= 1.4 \times 10^3$) is the molecular weight of the fragment oS of the oligomeric initiator oSLi. (This M_{oS} factor can be neglected at long t where $M(t)$ becomes much larger than M_{oS}). Thus, eq 11 is a nonlinear equation and the solution is obtained only numerically. (In the previous work,[25] the non-single-exponential decay of $\phi(t)$ was observed for PBLi in Bz but the deviation from the single exponential decay (from eq 3) was not very large. Thus, for PBLi, a perturbation calculation was made to calculate $\phi(t)$ analytically.[25] In contrast, the deviation is much larger for the hPSLi/dCH systems examined in this study (*cf.* Figure 4), and the perturbation calculation did not work well for these systems. Thus, we solved eq 11 numerically.)

For a given set of data summarized in Table I, $[I]_0$, C_{dPS}, $C_{hPS}(\infty)$, and $M_{hPS}(\infty)$ ($= M(\infty)$), we attempted to describe the $\phi(t)$ data in the absence/presence of dPS by choosing appropriate parameters included in eq 11, τ' ($= \{2/K_2\}^{1/2}/k_1$) and A_n ($= \{k_{2n}K''_n\}/\{2^{n-1/2}k_1K_2{}^{1/2}\}$) with $n \geq 2$. We considered up to the hexamer formation (up to A_3 in eq 11) in this attempt. The best results obtained with the parameter values, $\tau' = 19$ min mol$^{1/2}$ cm$^{-3/2}$, $A_2 = 1.8 \times 10^8$ mol$^{-3/2}$ cm$^{9/2}$, and $A_3 = 2.1 \times 10^{15}$ mol$^{-5/2}$ cm$^{15/2}$, are shown with the solid curves in Figures 4, 5, 8 and 9. The calculated results agree considerably well with the data for the middle-M_{hPS} batches with/without dPS, although deviations are noted for the low-M_{hPS} and high-M_{hPS} batches 4(0.02, 0), 148(0.11, 0), and 276(0.04, 0) in Figures 4 and 5. (The agreement for the middle-M_{hPS} batches became worse when we considered only the tetramer formation.) This result suggests that the non-single-exponential decay of $\phi(t)$ of the middle-M_{hPS} batches containing no dPS (Figures 4 and 5) and the retardation of the $\phi(t)$ decay due to dPS (Figures 8 and 9) can be consistently attributed to the osmotic interaction of the hPSLi aggregates with the other aggregates as well as with the dPS chains: This interaction suppresses the fusion of the dimers into larger aggregates, the latter possibly reacting with the hS monomers and contributing to the propagation. In the calculation, the concave shape of the $\log \phi(t)$ curve (Figure 4) and the increase of the $\{\log \phi(t)\}/t$ ratio with t (Figure 5) are prominently observed when this suppression is weak and strong, respectively, in the early and late stages of propagation in our experimental window, *i.e.*, for the batches having middle-M_{hPS} and fairly large $C_{hPS}(\infty)$ but without dPS. In the presence of semi-dilute dPS, the suppression occurs already in the early stage and the concave shape is not clearly observed. These features of the calculated $\phi(t)$ are in accordance with the data.

In relation to this conclusion, comments should be made for the deviation of the model calculation from the $\phi(t)$ data for the low-M_{hPS} batch 4(0.02,0) shown in Figures 4 and 5. The model assumed that the dimer is the *most stable* aggregate and thus non-reactive. This assumption is justified by the viscosity/scattering data in the range of $10^{-3}M_{hPS}$ between 11 and 160.[1–4,12] However, for smaller M_{hPS}, some bigger aggregates *could* be also stabilized, as suggested from the ^{1}N NMR/scattering data for low-M polybutadienyl lithium in heptane (showing a decrease of aggregation number with increasing $\phi(t)$ in the early stage of propagation).[16] If this is the case for the low-M_{hPS} chains in the batch 4(0.02,0), the bigger aggregates in this batch may be less reactive than considered in our calculation. For this case, the normalized propagation rate constants of these aggregates, A_n (eq 12), need to be set smaller than those giving the solid curves in Figures 4 and 5 ($A_2 = 1.8 \times 10^8$ mol$^{-3/2}$ cm$^{9/2}$ and $A_3 = 2.1 \times 10^{15}$ mol$^{-5/2}$ cm$^{15/2}$). *As a trial*, we retained A_3 (for hexamer) but adjusted A_2 (for tetramer) to be zero and re-calculated $\phi(t)$ for the batch 4(0.02,0). The resulting $\phi(t)$, shown with the dotted curve in the top left panels of Figures 4 and 5, agrees well with the data (circles). Of course, this adjustment of the A_2 value has not been justified experimentally. Nevertheless, this agreement suggests that the behavior of low-M_{hPS} batch 4(0.02,0) could be consistently explained within the model if the stability of the bigger aggregates therein is properly accounted for.

Comments should be also made for the deviation of the model calculation from the $\phi(t)$ data for the high-M_{hPS} batches 148(0.11,0) and 276(0.04, 0); see two bottom panels of Figures 4 and 5. Since the stability of the bigger aggregates can change with $\phi(t)$ only during the polymerization process of low-M_{hPS} chains (or only in the *very* early stage in the polymerization of middle-M_{hPS} and high-M_{hPS} chains), the deviation seen for those high-M batches at long t cannot be related to the stability change. One possible origin of this deviation is the slowing of the thermal motion of the high-M dimers and bigger aggregates that unequivocally occurs as the polymerization proceeds. The model implicitly assumes that the thermal collision of the dimers/bigger aggregates occurs much more frequently than the fusion of the dimers into larger reactive aggregates thereby considering only the osmotic

barrier in the fusion probability (the $\exp(-\Delta G_{os}^{[n]}(t)/k_BT)$ term in eq 11). Previous ^{7}Li NMR and viscosity experiments for low-M PBLi chains in Bz indicated validity of this assumption for these chains. This would be the case also for most of the hPSLi chains examined in this study, but not necessarily for the high-M_{hPS} hPSLi chains in the batches 148(0.11,0) 276(0.04, 0). If the motion of the high-M dimers/bigger aggregates affects the propagation in these batches, the propagation rate constants would considerably decrease with increasing t and $\phi(t)$ to result in the observed deviation. A test of this hypothesis is considered as an important subject of future work.

The simple kinetic model proposed in this study includes problems related to the stability of large aggregates (for the case of low-M_{hPS} chains) and the contribution of the chain/aggregate motion to the propagation (for the case of high-M_{hPS} chains), as explained above. In addition, the model does not consider the secondary effect of the shift of the unimer/dimer equilibrium on the propagation (the effect (3) explained earlier). Furthermore, the model is based on the simplifying assumption that the osmotic pressure of the anionic $2n$-mer aggregates is equal to that of the corresponding neutral hPS. Thus, the model is to be refined for these points. Nevertheless, the agreement between the model calculation and the $\phi(t)$ data for most of the systems strongly suggests that the propagation kinetics of hPSLi in dCH is strongly/mainly affected by the osmotic suppression of fusion of dimers into reactive, larger $2n$-mer aggregates.

CONCLUDING REMARKS

We have made ^{1}H NMR measurements to examine the propagation kinetics of hPSLi in a nonpolar solvent, dCH, mainly at 34.5 °C. The hPSLi chains form dimeric aggregates as the most stable aggregates. The residual monomer fraction $\phi(t)$ did not rigorously exhibit the single-exponential decay with t, which indicates the failure of the conventional molecular picture considering the propagation only through the dissociated unimer chains.

The observed non-single-exponential decay of $\phi(t)$ appears to be attributed to the propagation through large aggregates formed by transient fusion of the dimers. This fusion-aided propagation is osmotically suppressed on an increase of the hPS concentration and in the presence of a chemically inert dPS chains. The $\phi(t)$ data in the absence/presence of dPS were considerably well described by a simple kinetic model assuming the competitive propagation through the fused aggregates and dissociated unimers (although a deviation of the model calculation from the data for the low- and high-M hPSLi chains indicates a necessity of further refinement of the model). This result suggests an importance of the osmotic interaction (= polymeric character of growing chains) in the propagation kinetics of hPSLi in dCH.

Acknowledgment. This work was partly supported by Grant-in-Aid for Scientific Research on Priority Area "Soft Matter Physics" from the Ministry of Education, Culture, Sports, Science and Technology (grant #18068009).

Received: February 9, 2008
Accepted: May 7, 2008
Published: June 25, 2008

REFERENCES

1. M. Morton, "Anionic Polymerization: Principles and Practice." Academic Press, New York, 1983.
2. M. Szwarc, *Adv. Polym. Sci.*, **49**, 1 (1983).
3. M. Szwarc and M. van Beylen, "Ionic Polymerization and Living Polymers," Chapman and Hall, New York, 1993.
4. H. L. Hsieh and R. P. Quirk, "Anionic Polymerization," Marcel Dekker, New York, 1996.
5. M. Morton, E. E. Bostick, R. A. Livigni, and L. J. Fetters, *J. Polym. Sci. A*, **1**, 1735 (1963).
6. M. Morton and L. J. Fetters, *J. Polym. Sci. A*, **2**, 3311 (1964).
7. M. Morton, L. J. Fetters, R. A. Pett, and J. F. Meier, *Macromolecules*, **3**, 327 (1970).
8. H. L. Hsieh, *J. Polym. Sci. A*, **3**, 173 (1965).
9. H. L. Hsieh, *J. Polym. Sci. A*, **3**, 153 (1965).
10. A. F. Johnson and D. J. Worsfold, *J. Polym. Sci. A*, **3**, 449 (1965).
11. S. Bywater and D. J. Worsfold, *J. Organomet. Chem.*, **10**, 1 (1967).
12. D. J. Worsfold and S. Bywater, *Macromolecules*, **5**, 393 (1972).
13. L. J. Fetters, *J. Res. Natl. Bur. Stand. Sect. A*, **69**, 159 (1965).
14. J. M. Alvariño, A. Bello, and G. M. Guzman, *Eur. Polym. J.*, **8**, 53 (1972).
15. R. N. Young, R. P. Quirk, and L. J. Fetters, *Adv. Polym. Sci.*, **56**, 1 (1984).
16. A. Z. Niu, J. Stellbrink, J. Allgaier, L. Willner, D. Richter, B. W. Koenig, M. Gondorf, S. Willbold, L. J. Fetters, and R. P. May, *Macromol. Symp.*, **215**, 1 (2004).
17. L. J. Fetters, N. P. Balsara, J. S. Huang, H. S. Jeon, K. Almdal, and M. Y. Lin, *Macromolecules*, **28**, 4996 (1995).
18. J. Stellbrink, L. Willner, O. Jucknischke, D. Richter, P. Lindner, L. J. Fetters, and J. S. Huang, *Macromolecules*, **31**, 4189 (1998).
19. J. Stellbrink, L. Willner, D. Richter, P. Linder, L. J. Fetters, and J. S. Huang, *Macromolecules*, **32**, 5321, (1999).
20. A. Z. Niu, J. Stellbrink, J. Allgaier, L. Willner, A. Radulescu, D. Richter, B. W. Koenig, R. P. May, and L. J. Fetters, *J. Chem. Phys.*, **122**, 134906 (2005).
21. Y. Matsuda, T. Sato, Y. Oishi, and H. Watanabe, *J. Polym. Sci., Part B: Polym. Phys.*, **43**, 1401 (2005).
22. Y. Oishi, H. Watanabe, T. Kanaya, H. Kaji, and F. Horii, *Polym. J.*, **38**, 277 (2006).
23. A. Frischknecht and S. T. Milner, *J. Chem. Phys.*, **114**, 1032 (2001).
24. Y. I. Estrin and T. S. Zyubina, *Polym. Sci. Ser. A*, **42**, 1059 (2000).
25. Y. Oishi, Y. Matsumiya, and H. Watanabe, *Polym. J.*, **39**, 304 (2007).
26. P. Stepanek, R. Perzynski, M, Delsanti, and M. Adam, *Macromolecules*, **17**, 2340 (1984).
27. Aldrich Co. Catalogue Spec. ([1735-17-7] C_6D_{12}).
28. J. F. Rudd, *Physical Constants of Poly(Styrene)*, in "Polymer Handbook," J. Brandrup and E. H. Immergut Ed., 3rd Ed., Chapter V/81 Wiley, New York, 1989.
29. Y. Feng, R. A. Weiss, A. Karium, C. C. Han, J. F. Ankner, H. Kaiser, and D. G. Peiffer, *Macromolecules*, **29**, 3918 (1996).
30. Y. Miyaki, Y, Einaga, and H. Fujita, *Macromolecules*, **11**, 1180 (1978).
31. H. Watanabe, Y. Oishi, T. Kanaya, H. Kaji, and H. Horii, *Macromolecules*, **36**, 220 (2003).
32. J. I. Kaplan and A. N. Garroway, *J. Magn. Reson.*, **49**, 464 (1982).
33. Y. Higo, N. Ueno, and I. Noda, *Polym. J.*, **15**, 367 (1983).
34. I. Noda, Y. Higo, N. Ueno, and T. Fujimoto, *Macromolecules*, **17**, 1055 (1984).

